ECO-FRIENDLY SYNTHESIS OF SILVER NANOPARTICLES BY CHEMICAL REDUCTION METHOD

V. SUMAN[1,2,*], V. MORARI[2], L. GHIMPU[2], I. LUNGU[1], T. POTLOG[1], V. OSOIANU[3]

[1] Moldova State University, Doctoral School "Natural Sciences", Alexei Mateevici St 60, MD-2009, Chisinau, Republic of Moldova
[2] Technical University of Moldova, Institute of Electronic Engineering and Nanotechnologies, Academy St. 3/3, MD-2028, Chisinau, Republic of Moldova
[3] Vasili Levski Theoretical High School
[*] *Corresponding author*: victor.suman@iien.utm.md

Received October 8, 2024

Abstract: Silver nanoparticles were prepared by chemical reduction method. Silver nitrate was taken as metal precursor, chondroitin sulfate as stabilizing agent and glucose as reducing agent. The formation of AgNPc was monitored by UV-VIS absorption spectroscopy. UV-VIS spectroscopy revealed the formation of AgNPc by showing typical surface plasmon absorption maxima at 420-429 nm in the UV-VIS spectrum. Comparison of theoretical (Mie light scattering theory) and experimental data showed that the diameter of AgNPc in colloidal solution is about 20 nm. X-ray diffraction (XRD), FTIR spectroscopy and UV-VIS spectroscopy were used to characterize the obtained nanoparticles. The peaks in the XRD curves are in good agreement with the standard cubic shape values of metallic silver (JCPDS No. 04-0783) and no peaks of other crystalline impurity phases were detected.

Key words: nanoparticles, surface plasmon absorption, UV-VIS and FTIR spectroscopy.

DOI: https://doi.org/10.59277/RomJPhys.2025.70.607

1. INTRODUCTION

The study of nanoparticles (NPs) has become a promising tool for searching for new materials that can improve applications in various technologies, in particular, catalysis, optical and electronic devices. Silver NPs ($AgNO_3$) are among the extensively studied NPs, because they exhibit unique electrical, optical, mechanical, magnetic, and chemical properties that significantly differ from those of bulk materials, which depend on their size and shape, and are becoming extremely important for technological applications [1]. Recent studies have been focused on the synthesis of homogeneous silver NPs and the determination of their antimicrobial activity [2]. Metal particles in the nanometer size range have gained considerable interest in recent years, because they serve as building blocks of next-generation nanodevices. They have potential applications in surface-enhanced Raman spectroscopy, display devices, catalysts, microelectronics (light-emitting diodes and solar cells), and as biological diagnostic probes [3]. For this reason,

current research on nanostructured materials is mainly dedicated to understanding changes in the fundamental properties of matter at the nanoscale. The study of the mechanisms involved in the NP formation and growth process is of fundamental importance for understanding the chemical process and controlling the development of the NP microstructure. The application of modern spectroscopic techniques to study the microstructural evolution of metallic microclusters plays a major role in the chemistry of these materials, because it provides the possibility of *in situ* monitoring new reaction schemes for synthesizing nanometer clusters. Another important point concerns the reproducibility of the microcluster formation and growth process. Since the properties of nanostructured materials are strictly related to their microstructure (*i.e.*, shape, size, and composition), it is crucially important to know the effect of different experimental conditions on the synthesis process to provide the reproducibility of the reaction.

The surface morphology of the resulting nanomaterial is governed by the nature of the stabilizing agent, the molar ratio between the reducing agent and the silver salt, the redox potential, the stirring of the solvent, and the synthesis rate and temperature. Of all the above parameters, the stabilizer concentration is essential for the production of AgNPs. The use of $AgNO_3$ increases the possibility that nitrate (NO_3) is the dominant anion bound to the silver nanomaterial. The reducing agent can be any chemical agent, plant extract, or biological agent, such as H_2, gas, sodium borohydrin, hydrazine, ethanol, ethylene glycol, and ascorbic acid [4]. The simplest and most commonly used method for synthesizing metal NPs in a bulk solution is the chemical reduction of metal salts [5]. In fact, there are reports on the synthesis of nanosized metallic silver particles with different morphologies and sizes [6] using the chemical reduction of silver salts [3, 7]. This synthesis method involves the reduction of an ionic salt in a suitable medium in the presence of a surfactant using various reducing agents [8].

Silver NPs have attracted attention due to their unique ability to interact with electromagnetic radiation, while reducing a multitude of characteristics, in particular, surface plasmon resonance (SPR). This interaction imparts remarkable optical properties, electrical conductivity, and chemical stability to these NPs. These properties have paved the way for their use in diverse sectors, such as medical science, gene therapy, thermotherapy, and environmental improvement. Among the different methods to synthesize these NPs, especially for silver NPs, the “green” synthesis holds a unique position [19]. Numerous studies have shown the effectiveness of AgNPs against a variety of cancer cell lines and viruses. Nanosized Ag particles can easily penetrate into cells either by simple diffusion or by transporting through membranes, ion channels, or receptors [9].

Silver NP dispersions exhibit intense colors due to absorption induced by plasmon resonance. The surface of a metal is similar to a plasma, with free electrons in the conduction band and positively charged nuclei. Plasmon resonance is a collective excitation of electrons in the conduction band near the NP surface.

The electrons are confined to specific vibrational modes depending on particle size and shape. Therefore, metallic NPs have characteristic optical absorption spectra in the UV–VIS region [10, 18].

The aim of this study is to optimize the physical parameters for AgNP synthesis using chondroitin sulfate (ChS) and glucose. These preparations were chosen because they are commonly used in traditional medicine and are readily available. In addition, the optimized NPs were characterized and analyzed for antibacterial and hemolytic properties [16].

2. MATERIALS AND METHODS

This study was designed for the green synthesis of AgNPs. All chemicals used in this study were reagent grade materials. Chondroitin sulfate with a purity of 99% was purchased from Merck (Sigma Aldrich); glucose with a molar mass of 40000 was purchased from POCH S. A. (Poland), and $AgNO_3$ with a purity of 99.99% was also purchased from Merck (Sigma Aldrich). Chondroitin sulfate was used as a coating agent due to the excellent biocompatibility and biodegradability of this material. Chondroitin sulfate is an anionic polyelectrolyte with negatively charged sulfate and carboxylate groups.

2.1. SILVER NANOPARTICLE SYNTHESIS

The procedure for synthesizing AgNPs using ChS as a stabilizing agent and glucose as a reducing agent is relatively simple. The synthesis of silver NPs was run at a constant temperature of 40°C. In a beaker, 100 mg of glucose was dissolved with 80 mL of bidistilled H_2O; the resulting mixture was subsequently poured into a glass reactor equipped with a magnetic stirrer (Fig. 1).

Fig. 1 – Silver nanoparticle synthesis reactor.

The reactor was placed in a water bath, in which the temperature was maintained constant at T = 40°C and monitored with an accuracy of 0.1°C. Upon temperature stabilization over the glucose solution at 40°C, a ChS solution was slowly added. In a separate beaker, $AgNO_3$ was dissolved in 20 mL of bidistilled water. Upon temperature stabilization at 40°C, the $AgNO_3$ solution was slowly dripped into the reactor over the glucose–ChS solution. The resulting solution was continuously stirred by means of a magnetic stirrer to allow homogenization of the reagent mixture. At the selected temperature of 40°C, the synthesis reaction occurs slowly, and the liquid in the reaction apparatus changes from colorless to light brown in color no earlier than after 1 h. As a result of the synthesis reaction, transparent solutions ranging in color from light brown (2 h) to dark brown (24–48 h of synthesis) are formed (Fig. 2).

Fig. 2 – Colloidal silver solutions obtained by the method of chemical reduction of $AgNO_3$ with chondroitin sulfate. 200 – at the start of synthesis, 201 – 1 h, 202 – 2 h, 203 – 3 h, 204 – 4 h, 205 – 24 h, 206 – 48 h.

The conditions used to prepare AgNPs are shown in Table 1. The synthesis conditions are shown in the table where the molar concentration of $AgNO_3$, ChS and glucose, as well as the solution temperature throughout the synthesis are indicated.

Table 1

Synthesis conditions of AgNPs

Nr.	Temperature, °C	C_M, M		
		$A_g NO_3$, 10^{-3}	ChS, 10^{-3}	glucose, 10^{-3}
1	40	5.89	0.45	5.55
2	40	5.89	0.89	5.55
3	40	5.89	1.34	5.55
4	40	5.89	1.79	5.55
5	40	5.89	2.24	5.55

Sodium chloride was added to confirm the completeness of the reaction and verify the complete conversion of silver ions to AgNPs. The appearance of

opalescence in the reaction solution indicates the presence of silver ions, while a clear solution confirms the completion of the reaction. The total nanosilver content in the solutions was measured using the gravimetric method. The AgNPs were dissolved in a 10% nitric acid solution; after that, excess sodium chloride was added to the solution. The total amount of silver was determined by weighing the AgCl precipitate. Although most of the reduction is complete at a higher ChS concentration, only a small fraction of the Ag^+ ions is reduced at an equimolar concentration.

The encapsulating process was implemented under isothermal conditions using a thermostatic bath. The initial spectral data were not used in this study, because the extinction values are affected by the variation in the microcluster concentration (nucleation stage) and probably by a change in the diffusion coefficient (at the early stages of growth, the microclusters move toward the center of the coil between the particles); in addition, the analytical model is not really correct for extremely small microcluster sizes. Usually, this initial period is of short duration, depends on temperature and duration of synthesis. It was found that the growth rate calculated from spectrophotometric data increases linearly with the square root of the synthesis time, according to the law governing a typical diffusion-controlled process (Sugumoto 1987). Since the kinetic sequences were found to be localized on the same 48 h fitting curve, a high reproducibility of the microcluster growth process can be obtained under these conditions. In particular, it is well known that one of the main limitations in the synthesis of metal clusters by colloidal chemistry is the poor reproducibility of the nucleus growth process due to difficulties in precisely controlling the various physical or chemical parameters involved in the reaction (*e.g.*, reagent purity, reactor wall surface characteristics, stirring speed, etc.). However, a poor reproducibility of the kinetic data is mainly due to the fact that the ChS protective layer, which controls the diffusion rate of silver atoms toward the surface of the growth nucleus, requires a certain time to reach thermodynamic equilibrium. The ChS layer encapsulating the growing microclusters evolves dynamically by absorbing the solvent during growth until it reaches thermodynamic equilibrium. Therefore, to achieve a high reproducibility of the diffusion process and, consequently, the particle growth rate, the protective layer should be at thermodynamic equilibrium during the nucleation and growth of the microcluster and during the aging of the ChS protective solution and can be explained on the basis of an increase in the barrier to ChS, which in turn enhances the diffusion of silver atoms through the barrier. After 48 h of synthesis, the radial growth of microclusters always exhibits the same behavior, because under these conditions the thermodynamic equilibrium is finally observed.

2.2. COLLECTING SILVER NANOPARTICLES

Excess unreacted ChS and silver ions remaining in suspension were separated from the ChS-AgNPs nanoparticles using a sedimentation device by centrifugation at 3000 rpm for 15 min. At the end of the centrifugation process the AgNPs sediment to

the bottom of the vial and the solution becomes transparent, which is illustrated in Fig. 3.

Fig. 3 – Vial with sedimented nanoparticles after centrifugation.

The AgNPs prepared by this method were purified initially with bidistilled water and then with a 50/50 ethyl alcohol–acetone solution. Finally, the AgNPs were dried in an oven at 40°C. Figure 4 shows the synthesized AgNPs. The synthesized silver powders are highly soluble in water to form stable colloidal solutions.

Fig. 4 – Synthesized silver NPs.

2.3. OPTIMIZATION OF DIFFERENT PARAMETERS FOR AgNP SYNTHESIS

The parameters (time, pH, temperature, and concentrations of silver nitrate, glucose, and ChS) were optimized for rapid and maximum synthesis of AgNPs. The pH was maintained at 2, 4, 6, and 8 and adjusted with sodium hydroxide (NaOH). The synthesis reaction was monitored in a range of 0–48 h for the optimum synthesis of AgNPs. The synthesis of silver NPs was monitored at different encapsulating temperatures (30, 40, 50°C). The silver nitrate concentration was optimized at different concentrations (0.5, 1.0, 1.5, 2.0 mM). Similarly, the concentration ratio of ChS, glucose, and $AgNO_3$ was optimized by increasing the ChS concentration in a 1 mM $AgNO_3$ solution. Synthesis was observed at different ratios of ChS, glucose, and silver

nitrate solution. Absorption of the NPs was observed in a range of 300–800 nm using a UV–VIS spectrometer.

3. RESULTS AND DISCUSSION

3.1. ULTRAVIOLET–VIS SPECTROSCOPY

The visible color change from light brown to dark brown indicated the formation and nucleation of silver NPs. The appearance of the dark brown color can be attributed to the vibrational effect of the surface plasmon and the replacement of Ag^+ ions by Ag^0 under the action of ChS. The optical characteristics of the AgNPs extracted at different stages of their synthesis from ChS–glucose–$AgNO_3$ were studied by UV–VIS spectroscopy and represented as absorption spectra. These spectra are shown in Fig. 5, which shows that the absorption intensity of the colloidal solution of AgNPs increases with increasing reaction time. The lowest spectrum corresponds to 2 h of reaction, while the spectrum with the maximum intensity corresponds to 48 h of reaction. In addition, Fig. 5 shows that the position of the absorption band of the surface plasmon of nanosized silver is shifted toward longer wavelengths during the synthesis reaction.

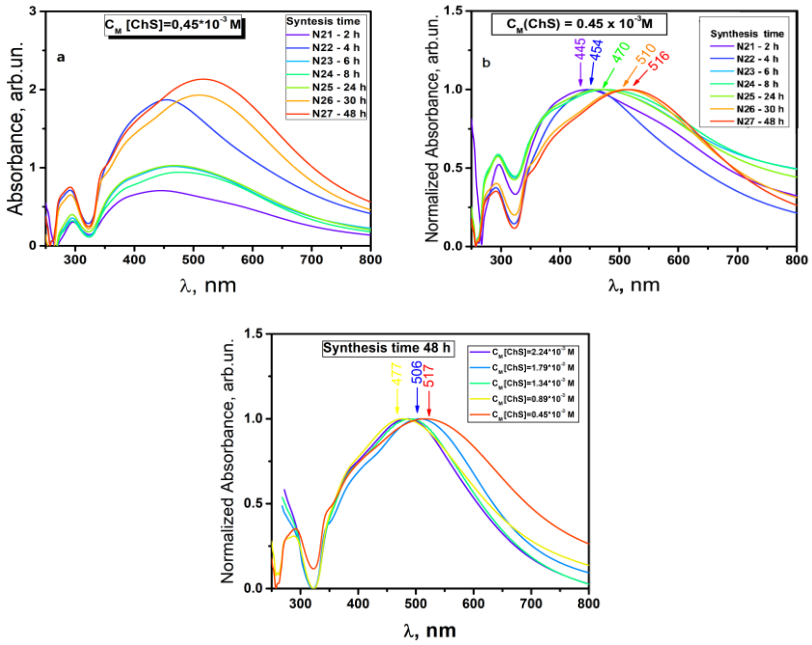

Fig. 5 – Ultraviolet–Vis spectra of colloidal solutions of AgNPs obtained at expected synthesis time intervals (a, b) and different ChS concentrations at 48 h (c).

The increase in absorption intensity with increasing reaction time can be associated with an increase in the AgNP size, which is shown in Fig. 6.

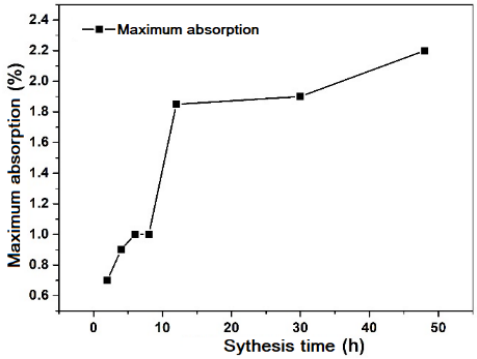

Fig. 6 – Maximum uptake as a function of synthesis time.

Absorption of silver ions at the NP–solution interface also shifts the position of the plasmon absorption spectrum toward longer wavelengths, especially for silver NPs smaller than 10 nm. Under the synthesis conditions used in this work, silver species can be adsorbed by the newly formed NPs and then undergo reduction at the solid–solution interface.

Two absorption maxima are observed in the optical absorption spectra (Fig. 5). Based on literature data [13] it can be concluded that the first peak corresponds to the absorption maximum of ChS at a wavelength of 298 nm. An increase in the ChS concentration leads to an increase in absorbance. In addition, a change in the peak shape is observed; it indicates the involvement of ChS in the reduction of $AgNO_3$. The second peak corresponds to the absorption maximum of silver NPs at a wavelength of 454 nm.

The optical properties of the colloidal nanosilver solutions were studied by UV–VIS spectroscopy and plotted in Fig. 7.

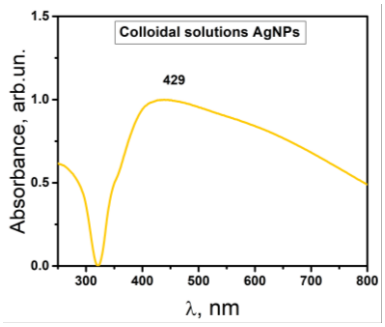

Fig. 7 – Ultraviolet–VIS absorption spectra of silver NPs dispersed in bidistilled water for AgNPs–ChS.

The UV–VIS spectra reveal the formation of silver NPs according to the appearance of an SPR at 429 nm for AgNPs–ChS. The position and shape of plasmonic absorption depend on particle size, shape, and dimension. This is in agreement with the study by Mock J.I. *et al.* [14] who showed a correlation between the absorption spectra of silver NPs and their size (20–100 nm) and shape (spheres, decahedra, triangular pyramids). These studies showed that spherical and nearly spherical NPs absorb in the blue, green, and red regions of the spectrum, respectively.

3.2. FOURIER TRANSFORM INFRARED (FTIR) ANALYSIS

The intermolecular interaction and the nature of the chemical bonding in the resulting system were studied by FTIR. Figure 8 shows the FTIR spectra of $AgNO_3$ and AgNPs–ChS.

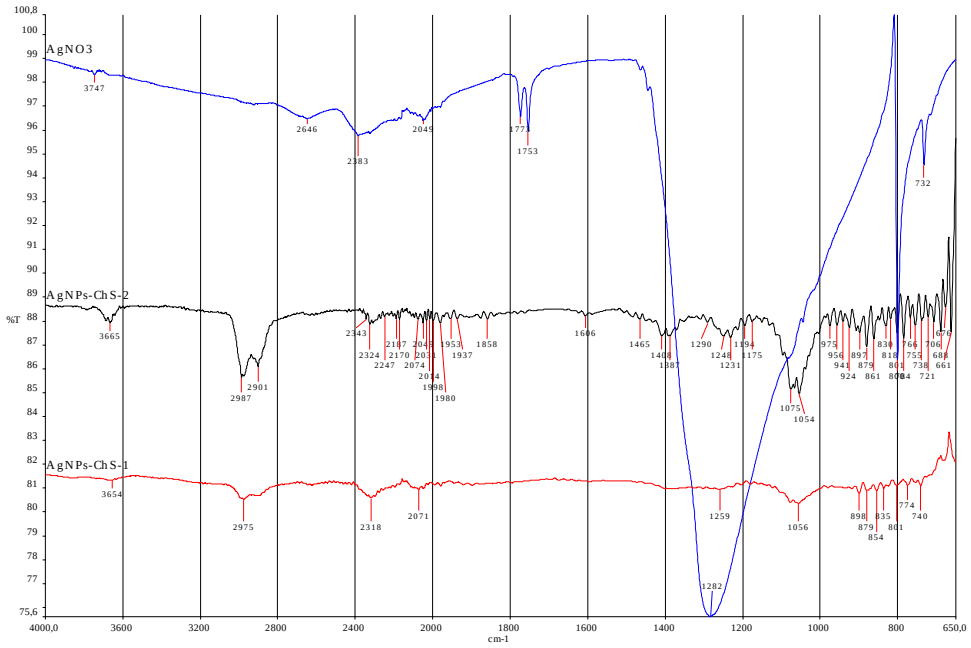

Fig. 8 – Fourier transform infrared spectra of $AgNO_3$ and AgNPs after reduction and ChS coating.

The AgNPs powder was analyzed by FTIR spectroscopy to obtain valuable information about the functional groups involved in the reduction of silver ions. The use of ChS and glucose as reducing and stabilizing agents was studied by FTIR spectroscopy, which makes it possible to identify the functional groups attributed to these substances. The FTIR spectra were recorded for powders of $AgNO_3$, glucose, and AgNPs after reduction and coating with ChS. The FTIR spectrum of $AgNO_3$ exhibits characteristic bands of the nitrate group, which are localized at 1280, 1052,

and 798 cm^{-1}. The band at 1280 cm^{-1} is slightly shifted relative to the typical range of the asymmetric stretching vibrations of the nitrate group (1380–1410 cm^{-1}). This difference can be attributed to the effect of the crystal structure or intermolecular interactions. The band at 1052 cm^{-1} fits well into a range of 1040–1060 cm^{-1} for the symmetric stretching vibrations of the NO_3^- group. The band at 798 cm^{-1} is attributed to the bending vibrations of the NO_3^- group.

The FTIR spectrum of glucose represents the complex structure of this material with multiple hydroxyl groups, C–H bonds, and interactions between ether and cyclic bonds, with bands identified at 3236, 2936, 1371, 1332, 1153, 1026, 1009, 851, 768, 713, and 510 cm^{-1}. The band at 3236 cm^{-1} is attributed to the O–H stretching vibrations. The band at 2936 cm^{-1} corresponds to the C–H stretching vibrations. The band at 1371 cm^{-1} is assigned to the C–H bending vibrations in the methyl (CH_3) and methylene (CH_2) groups. The band at 1332 cm^{-1} can be attributed to the O–H bending vibrations in hydroxyl groups or represent other modes of the C–H bond vibrations. The band at 1153 cm^{-1} and the band at 1026 cm^{-1} correspond to the C–O and C–OH stretching vibrations. The band at 1009 cm^{-1} is attributed to the C–O–C and C–OH vibrations in the glucose structure. The band at 851 cm^{-1} is assigned to the C–H bond and cyclic bond stretching vibration modes in the glucose structure. The band at 768 cm^{-1} can be attributed to the pyran ring bending vibrations or other C–H bond vibrational modes. The band at 713 cm^{-1} is assigned to the planar bending vibrations of the C–H bond or vibrational modes associated with the ring structure. The band at 510 cm^{-1} can be attributed to the bending vibrational modes of the molecular skeleton.

In the FTIR spectrum of ChS, the band at ~3400 cm^{-1} is attributed to the O–H stretching vibrations of the hydroxyl (–OH) groups present in ChS. The band at ~1650 cm^{-1} corresponds to the C=O stretching vibrations in the carboxyl (–COOH) groups and in the glycosaminoglycan structure. The band at ~1250 cm^{-1} is assigned to the S=O stretching vibrations of the sulfate groups ($–SO_4^{2-}$) present in ChS. The band at ~1150 cm^{-1} corresponds to the C–O and C–O–S stretching vibrations of the ether and sulfate groups. The band at ~820 cm^{-1} is assigned to the C–O–S and C–O–H bending vibrations. The band at ~750–800 cm^{-1} can be attributed to the C–H bending vibrations and other vibrational modes characteristic of the ChS structure. The band at ~570–600 cm^{-1} can be assigned to the bending vibrations of the molecular skeleton and bonding groups.

In the FTIR spectra of AgNPs synthesized using glucose, $AgNO_3$, and ChS, bands localized at 3675, 2981, 2909, 1451, 1395, 1244, 1063, and 882 cm^{-1} were identified. The band at 3675 cm^{-1} is assigned to the O–H stretching vibrations of free hydroxyl (OH) groups. The band at 2981 cm^{-1} is attributed to the asymmetric C–H stretching vibrations. The band at 2909 cm^{-1} is similar to the band at 2981 cm^{-1}; this band corresponds to the symmetric C–H stretching vibrations. The band at 1395 cm^{-1} is attributed to the C–H bending vibrations and can be associated with the stretching vibrations of the sulfate groups. The band at 1244 cm^{-1} is assigned to

the S=O stretching vibrations of the sulfate groups. The band at 1063 cm^{-1} corresponds to the C–O and C–O–C stretching vibrations. The band at 882 cm^{-1} is attributed to the C–H bond bending vibrations.

Comparative analysis of the bands identified in the FTIR spectra of AgNPs with those of ChS, glucose, and $AgNO_3$ shows that most of the bands are in good agreement with those observed in the ligands used (ChS and glucose); however, there are some shifts, which can represent specific interactions and structural changes caused by the synthesis of silver NPs. Shifts toward higher frequencies (3675 cm^{-1}) suggest strong interactions of hydroxyl groups with the NPs. Slight shifts in the bands for C–H (2981 and 2909 cm^{-1}) indicate changes in the chemical environment of the C–H groups. The good agreement of the bands of the sulfate and NO_3^- groups (1244 cm^{-1}) suggests that functional groups are present and interact with the NPs.

3.3. X-RAY DIFFRACTION (XRD) ANALYSIS

The XRD patterns confirm the formation of crystalline metal NPs with the presence of coating agents on the NP surface. X-ray diffraction analysis is an extremely useful tool to study the characteristics, crystallization, and structure of the nanostructure. Figure 9 shows the XRD pattern peaks at 2θ = 38.24°, 44.20°, 64.73°, and 77.73°, which correspond to the cubic structure of Miller indices (111), (200), (220), and (311) of *hkl* values (JCPDS No. 04-0783) and are characteristic of metallic silver.

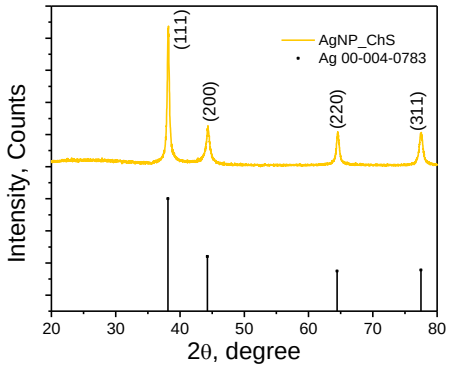

Fig. 9 – X-ray diffraction pattern of AgNPs–ChS.

The crystallite size can be calculated using the Scherrer equation:

$$D = 0.9\,\lambda / \beta\cos\theta \qquad (1)$$

where λ is the X-ray wavelength of 0.1541 nm (Cu), β is the full width at half maximum (FWHM) of the peak, θ is the diffraction angle, and *D* is the average

crystallite size. Scherrer formula (1) gives a rough estimate of the crystallite size and assumes that the peak broadening is attributed exclusively to the small crystallite size. Other factors, such as instrument effects and deformation, can also contribute to the peak broadening and should be taken into account for more accurate measurements. Results of studying the sample using the XRD pattern to measure the size of the synthesized NPs are shown in Table 2.

Table 2

Parameters of crystallites characterized by XRD analysis

Angle (Θ) in degrees	cosΘ	β (FWHM) in radians	λ (nm)	*D* (crystallite size) in nanometers
19.12	0.945	0.006829	0.1541	21.49

After calculating the FWHM of the curve using the original software, the average size of the synthesized NPs is about 21.49 nm. The peak intensity represents the high degree of crystallinity of the AgNPs.

4. APPLICATION

Metal NPs are characterized by a high surface area for strong adsorption and high reducibility, which can be used for biomedical applications, which include antibacterial, anticancer, and antioxidant activities and drug delivery mechanisms [15]. This "green" approach to synthesizing AgNPs is innovative and provides a valuable contribution to photodynamic therapy for treating cancer cells by functionalization of the metal phthalocyanine ZnPc with silver nanoparticles: $ZnPc(SO_3)_4$ chitosan/$AgNP_s$ [16] and $ZnPc(SO_3)_4$ChS/$AgNP_s$ [17].

5. CONCLUSIONS

In this study, a single-step environmentally friendly synthesis of AgNPs has been developed. The synthesis is run in a stirred aqueous environment at $T = 40°C$ using ChS as a stabilizing agent and glucose as a reducing agent. The reaction temperature, reaction time, and ChS concentration had obvious effects on the amount of AgNPs formed and the distribution of the NPs. Chemical reduction of silver species in a ChS–glucose–$AgNO_3$ solution at $T = 40°C$ yields monodispersed AgNPs with an average NP size of 21.49 nm. The UV–VIS spectra indicate that the position of the surface plasmon absorption peak of the AgNPs colloids is shifted from 464 nm at 2 h after the start of the synthesis process to 471 nm. This redshift in the absorption spectra of AgNPs is attributed to an increase in particle size, a process that can involve the reduction of absorbed Ag^- at the particle–solution interface.

Such a reduction of Ag- at the silver surface is the metal reduction potential lowering facility also mentioned by the authors Zeena S. *et al.* [20]. Comparative analysis of the bands identified in the FTIR spectra of AgNPs with those of ChS, glucose, and $AgNO_3$ shows that most of the bands are in good agreement with those observed for the ligands used; however, there are some shifts, which can represent specific interactions and structural changes caused by the synthesis of AgNPs. X-ray diffraction confirms the presence of a signal of elemental silver; no peaks of other impurities are detected. The result indicates that the synthesized product consists of high-purity AgNPs. These data of ChS-doped AgNPs are compared with AgNPs prepared by the green method; it is evident that the coating agents for the NPs are different for different reducing agents. Therefore, we can control the specific characteristics of our NPs by controlling the type of coating agent and the synthesis method used.

Acknowledgements. This work was supported by the project "Design of supramolecular architectures based on metal phthalocyanine derivatives – functionalized nanoparticles for medicine" (PAS FM-NP, code: 011209) supervised by Dr. Tamara POTLOG. The authors thank the team of the Scientific Research Laboratory "Advanced Materials in Biopharmaceutics and Engineering" of the State University of Moldova, Republic of Moldova.

REFERENCES

1. A. Braun, J. Tchernaic, *Uber die producte der einwirkung von acetanhydrid auf phthalamid*, European Journal of Inorganic Chemistry T **40** (2), 2709–2714 (1907).
2. Maribel G. Guzmán, Jean Dille, Stephan Gode, *Synthesis of silver nanoparticles by chemical reduction method and their antibacterial activity*, World Academy of Science Engineering and Technology International Journal of Materials and Metallurgical Engineering **43**, 357–364 (2008).
3. A. Kumar, H. Jochi, A. Mandole, M. Sastry, Journal of Colloid and Interface Science **264**, 396 (2003). https://doi.org/10.1016/S0021-9797(03)00567-8
4. A. El-Badawy, D. Feldhake, R. Venkatapathy, State of the Science Literature Review: Everything Nanosilver and More Environmental Protection Agency Washington DC USA 5-147 (2010).
5. A. Pal, S. Shah, S. Devi, Colloids and Surface A **302**, 51–57 (2007). https://doi.org/10.1016/j.colsurfa.2007.01.054
6. Z. Chen, L. Gao, Materials Research Bulletin **42**, 1657–1661 (2007). https://doi.org/10.1016/j.materresbull.2006.11.028
7. D. G. Li, S. H. Chen, S. Y. Zhao, X. M. Hou, X. G. Yang, Thin solid Films **460**, 78–82 (2004). https://doi.org/10.1016/j.tsf.2004.01.086
8. H. M. Abuzeid, C. M. Julien, L. Zhu, A.M. Hashem, *Green Synthesis of Nanoparticles and Their Energy Storage, Environmental, and Biomedical Applications*, Crystals **13**, 1576 (2023). https://doi.org/ 10.3390/cryst13111576.
9. G. Wang, C. Shi, N. Zhao, X. Du, *Synthesis and characterization of Ag nanoparticles assembled in ordered array pores of porous anodic alumina by chemical deposition*, Mater. Lett **61**, 3795–3797 (2007). https://doi.org/10.1016/j.matlet.2006.12.035
10. C.F. Bohren, F. Craij, *Absorption and Scattering of Light by Small Particles*, PC 882 B **63**, 533 (1983). https://doi.org/10.1002/9783527618156.ch3

11. U. Kreibig, M. Vollmer, *Optical properties of Metal Clusters*, Springer Berlin Heidelberg 535 (1995). https://doi.org/10.1007/978-3-662-09109-8
12. A. Henglein, *Colloidal Silver Nanoparticles: Photo-chemical Preparation and Interaction with O2 CCl and Some Metal Ions*, Chemistry of Materials **10**, 444–450 (1998) https://doi.org/10.1021/cm970613j
13. J. I. Mock, M. Barbic, D. R. Smith, D. A. Schultz, S. Schultz, *Shape effects in plasmon resonance of individual colloidal silver nanoparticles*, J. Chem. Phys. **116**, 6755–6759 (2002). https://doi.org/10.1063/1.1462610
14. A. I. Osman, Y. Zhang, M. M. Farghali *et al.*, *Synthesis of green nanoparticles for energy, biomedical, environmental, agricultural, and food applications*, Environ. Chem. Lett. **22**, 841–887 (2024). https://doi.org/10.1007/s10311-023-01682-3.
15. V. Suman, T. Potlog, I. Lungu, D. Untila, E. Stratulat, M. Diru, *Photophysical Properties of ZnPc(SO$_3$)$_4$ chitosan/AgNP$_s$ systems*, 10th International Conference on Materials Science and Condensed Matter Physics, 1–4 October, Chisinau (2024).
16. V. Suman, L. Ghimpu, I. Lungu, T. Potlog, *Synthesis of colloidal AgNP-substituted ZnPc systems and their antimicrobial activity*, International Conference NANO-2024 "Quo-Vadis-Ethics of the Scientific Research" 14–18 April Chisinau, Moldova, 2024.
17. Marcela-Elisabeta Barbinta-Patrascu, Cornelia Nichita, Bogdan Bita and Stefan Antohe, *Biocomposite Materials Derived from Andropogon halepensis: Eco-Design and Biophysical Evaluation*, Materials **17**, 1225 (2024). https://doi.org/10.3390/ma17051225.
18. Monica Mironescu, Andrada Lazea-Stoyanova, Marcela Elisabeta Barbinta-Patrascu, Lidia-Ioana Virchea, Diana Rexhepi, Endre Mathe and Cecilia Georgescu, *Green Design of Novel Starch-Based Packaging materials Sustaining Human and Environmental Health*, Polymers **13**, 1190 (2021). https://doi.org/10.3390/polym13081190
19. Zeena S. Pillai and Prashaut V. Kamat, *What factor control the size and shape of silver nanoparticles in the citrate ion reduction method*, J. Phys. Chem. B **108**, 945–951 (2004). https://doi.org/10.1021/jp037018r.